Supporting Information

Iron-induced formation of hierarchical open-cell hard carbon rich in oxygen functional groups for high-performance sodium ion storage

Liyuan Li, †*[ab] Fenglian Gong, †[b] Huilin Li,[b] Chenyang Guo,[b] Jiaoyan Wang,[b] Yan Zhang[b]

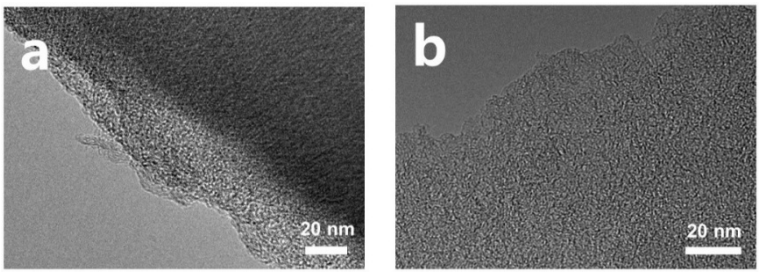

Figure S1. TEM images of a) JM and b) JM-Fe.

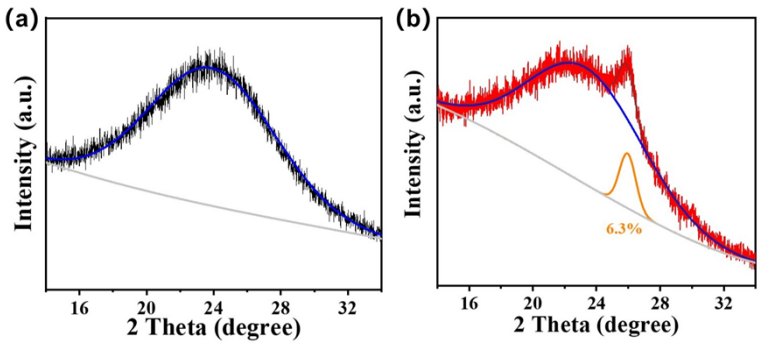

Figure S2. (a) Deconvolution of XRD patterns of (a) JM and (b) JM-Fe.

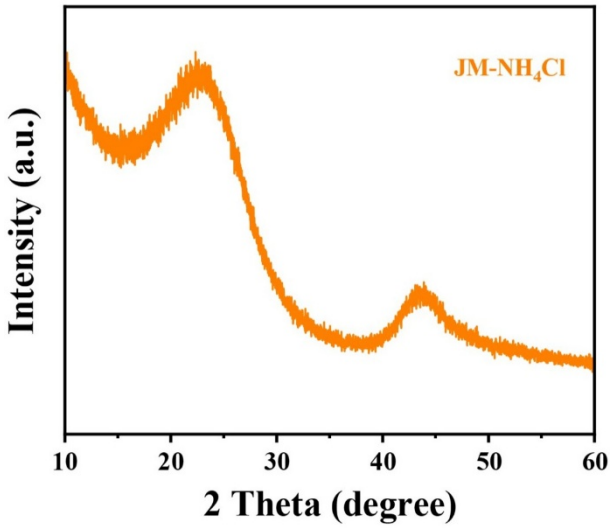

Figure S3. XRD pattern of JM-NH_4Cl.

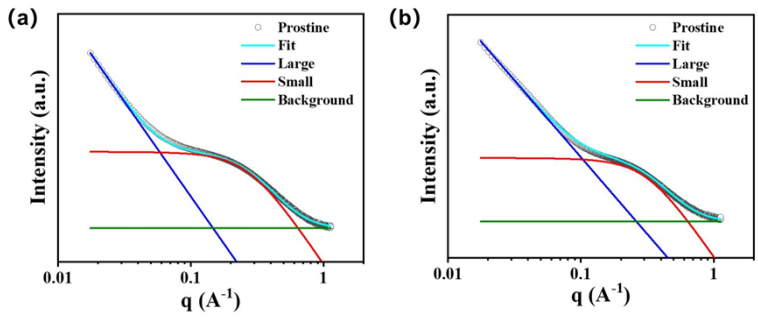

Figure S4. Fitted SXAS patterns. (a) SXAS patterns of JM. (b) SXAS patterns of JM-Fe.

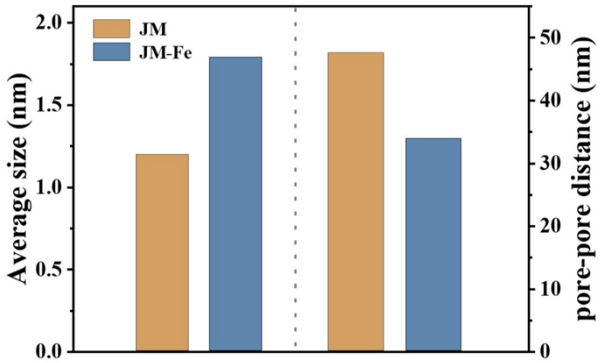

Figure S5. The average sizes and Pore-pore dimension for JM and JM-Fe.

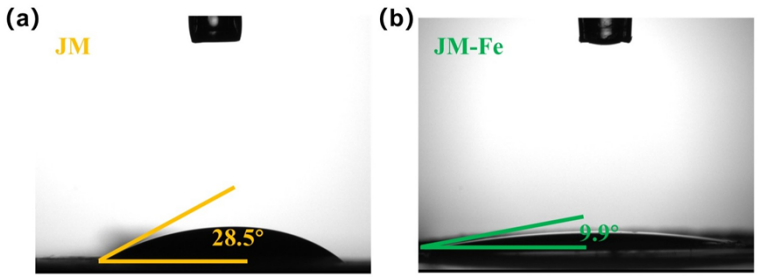

Figure S6. Electrolyte contact angle test of the JM and JM-Fe.

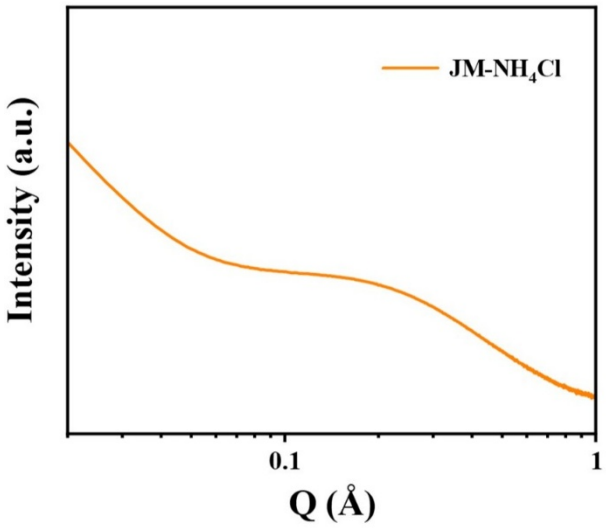

Figure S7. Small-angle X-ray scattering (SAXS) pattern of JM-NH_4Cl.

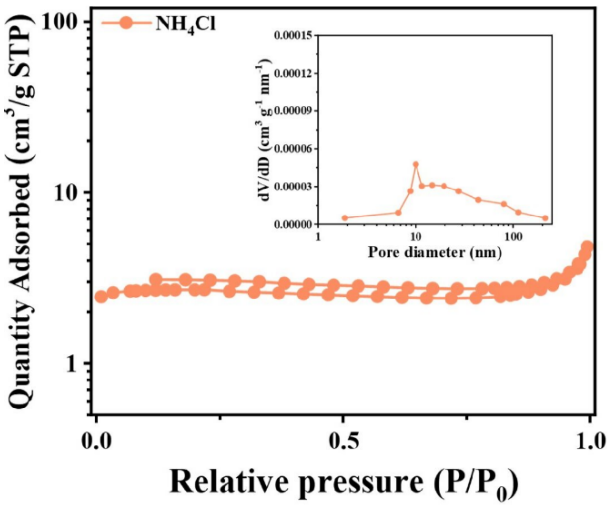

Figure S8. N_2 adsorption/desorption isotherm and Pore size distribution of JM-NH_4Cl.

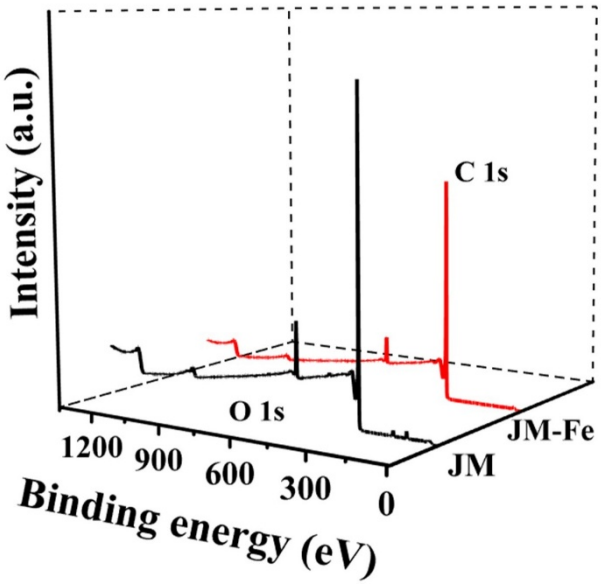

Figure S9. The survey spectra in JM and JM-Fe.

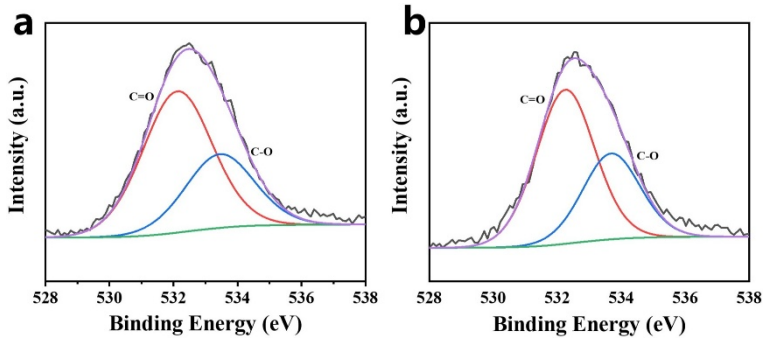

Figure S10. The survey spectra in JM and JM-Fe.

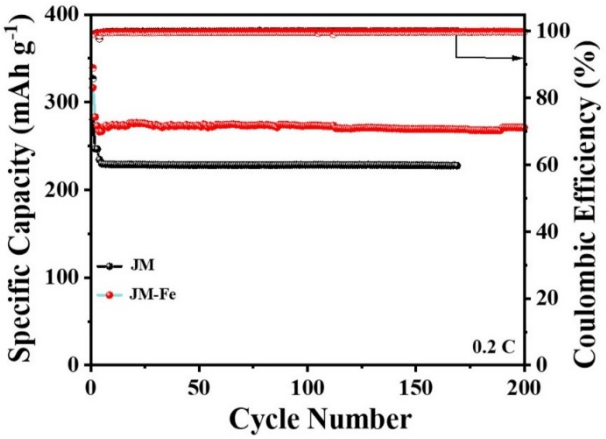

Figure S11. Cycling performance at 0.2 C of JM and JM-Fe.

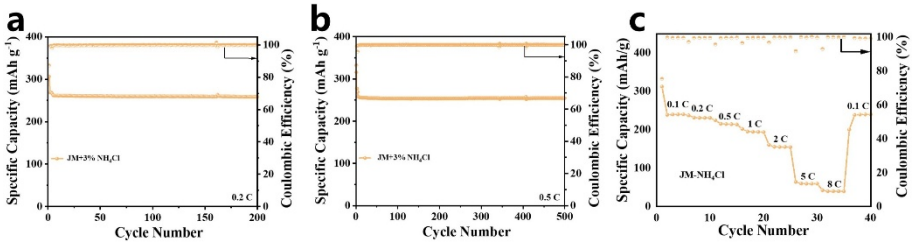

Figure S12. Cycling performance at a) 0.2 C and b) 0.5C of JM-NH_4Cl. c) Rate capability of JM-NH_4Cl.

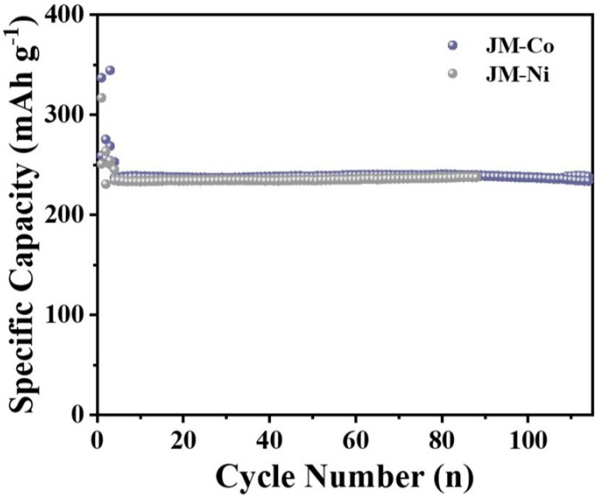

Figure S13. Cycling performance at 0.5 C of JM-Ni and JM-Co.

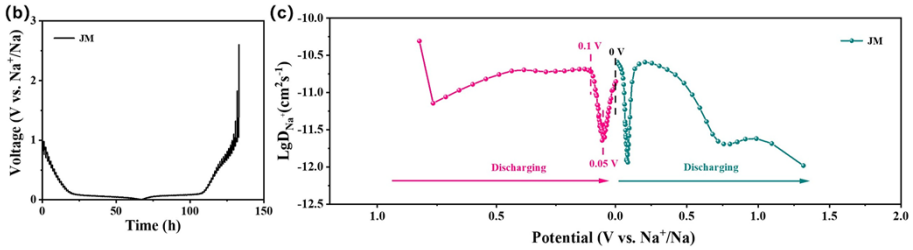

Figure S14. (a) GITT curve of JM and (b) Na^+ diffusion coefficient through discharging/charging process.

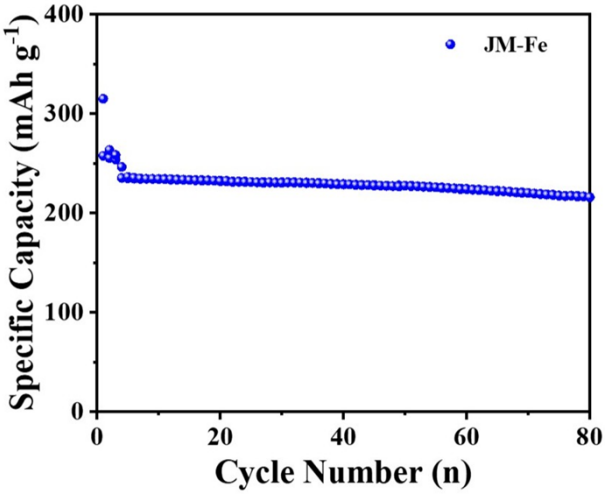

Figure S15. Cycling Performance of the JM-Fe at 0.5 C in Ester-Based Electrolytes.

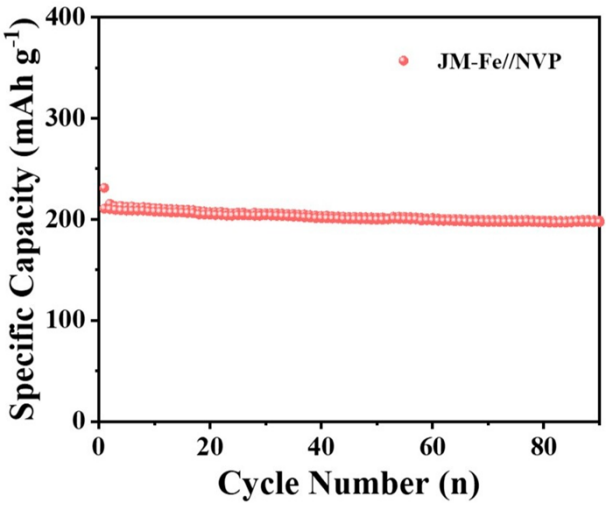

Figure S16. The cycling performance of NVP//JM-Fe full-cell tested at 0.5 C.

Table S1. Data extracted from various analyses

Materials	S_{BET} ($m^2 g^{-1}$)	Pore volume ($cm^3 g^{-1}$)	Average pore size (nm)	I_D/I_G	d(002) (nm)	Initial discharge capacity ($mAh g^{-1}$)	Sloping capacity ($mAh g^{-1}$)	Plateau capacity ($mAh g^{-1}$)
JM	12.8	0.011	3.42	1.02	0.369	320.0	139.6	180.4
JM-Fe	67.6	0.059	3.51	0.98	0.387	297.4	126	171.4